# Design and experimental validation of a high voltage ratio DC/DC converter for proton exchange membrane electrolyzer applications

Stefania Maria Collura, Damien Guilbert, Gianpaolo Vitale, Massimiliano Luna, Francesco Alonge, Filippo d'Ippolito, Angel Scipioni

# Design and Experimental Validation of a High Voltage Ratio DC/DC Converter for Proton Exchange Membrane Electrolyzer Applications

Stefania Maria Collura[a], Damien Guilbert[b,*], Gianpaolo Vitale[c], Massimiliano Luna[d], Francesco Alonge[a], Filippo D'Ippolito[a], Angel Scipioni[b]

[a] Università degli studi di Palermo, Dipartimento dell'Energia, Ingegneria dell'Informazione e Modelli Matematici (DEIM), Viale delle Scienze snc, 90128 Palermo, Italy

[b] Université de Lorraine, IUT de Longwy, Group of Research in Electrical Engineering of Nancy (GREEN), Longwy, France

[c] ICAR, Institute for high performance computing and networking, Italian National Research Council of Italy, Palermo, Italy

[d] INM, Institute for Marine Engineering, Italian National Research Council of Italy, Palermo, Italy

*corresponding author. Phone: +33372749984

e-mail: damien.guilbert@univ-lorraine.fr

*Abstract*

This paper deals with hydrogen production via water electrolysis, which is considered the most attractive and promising solution. Specifically, the use of renewable energy sources, such as wind electric power generators, is hypothesized for supplying the electrolyzer, aiming to strongly reduce the environmental impact. In particular, micro-wind energy conversion systems (μWECSs) are attractive for their low cost and easy installation. In order to interface the μWECS and the electrolyzer, suitable power conditioning systems such as step-down DC-DC converters are mandatory. However, due to the requested high conversion ratio between the DC bus grid, i.e. the output of a three-phase diode rectifier connected to the output of the electric generator, and the rated supply voltage of the electrolyzer, the classic buck converter alone is not suitable. Therefore, a converter is proposed and designed, consisting of a buck converter, a full-bridge IGBT converter, a single-phase transformer, and a diode bridge rectifier; LC filters are also included between buck and full-bridge converters, and at the output of the diode bridge rectifier with the aim of reducing the ripple on currents and voltages. The components of the described physical system from the output of the three-phase rectifier up to the electrolyzer are then modeled assuming the transformer as ideal, and the model is employed for designing a PI-type controller. Experimental results are provided in order to demonstrate the effectiveness of the developed converter and its control for these applications.

*Keywords*

Electrolyzer, DC/DC converter, Wind energy, High conversion ratio, Control technique, Modeling.

## NOMENCLATURE

*Acronyms*

| | |
|---|---|
| EL | electrolyzer. |
| FBC | full-bridge converter. |
| FC | fuel cell. |

| | |
|---|---|
| HBC | half-bridge converter. |
| HFT | high-frequency transformer. |
| Mg | magnesium. |
| PEM | proton exchange membrane. |
| PMSG | permanent magnet synchronous generator. |
| SO | solid oxide. |
| Ti | titanium. |
| WECS | wind energy conversion system. |

## *Roman symbols*

| | |
|---|---|
| A | attenuation (db). |
| B | bandwidth (Hz). |
| d | duty cycle. |
| $E_{elec}$ | counter electromotive force of the electrolyzer (V) |
| $f_{sw}$ | switching frequency (Hz). |
| i | current flowing trough $L_1$ (A). |
| $i_0$ | current flowing trough $L_3$ (A) |
| $i_2$ | current flowing trough $L_2$ (A) |
| $i_{1T}$ | tranformer input current (A). |
| $i_{2T}$ | tranformer output current (A). |
| $i_B$ | input current of full-bridge converter (A) |
| $i_{el}$ | current at the input of electrolyzer (A) |
| m | margin. |
| N | turns ratio of the transformer. |
| $R_1$ | resistance of the electrolyzer (Ω) |
| $r_{c1}$ | parasitic resistance of capacitor $C_1$ (Ω) |
| $r_{c2}$ | parasitic resistance of capacitor $C_2$ (Ω) |
| $r_i$ | current ripple (A). |
| $r_{L1}$ | parasitic resistance of inductor $L_1$ (Ω) |
| $r_{L2}$ | parasitic resistance of inductor $L_2$ (Ω) |
| $r_v$ | voltage ripple (V). |
| $T_{sw}$ | switching period (s). |
| $V_B$ | input voltage of full-bridge converter (V) |
| $v_{c1}$ | voltage across $C_1$ (V). |
| $v_{c2}$ | voltage across $C_2$ (V). |
| $v_{c3}$ | voltage across $C_3$ (V). |
| $v_{1t}$ | transformer input voltage (V). |

$v_{2t}$ transformer output voltage (V).

$\omega_c$ crossover frequency (rad.s$^{-1}$).

$\omega_r$ resonance frequency (rad.s$^{-1}$).

*Greek symbols*

$\varphi$ phase angle (°)

*Subscripts and superscripts*

g gain.

## 1. INTRODUCTION

Over the last decades, reserves of fossil fuels (e.g. oil, natural gas) have been depleting due to the growing demand [1]. Indeed, fossil fuels are widely used for diverse applications, especially in transportation and electricity production [2]. Their increasing use all over the world leads up to the large release of greenhouse gases, responsible for global warming and hazardous meteorological phenomena [1]. Based on the current reserves and fossil fuels production [3], oil and natural gas should be depleted during the 21$^{st}$ century (forecast exploitation time around 50 years). Hence, new energy solutions must be developed to face the depletion of fossil fuels and global warming.

Among the envisaged solutions, hydrogen is considered a promising solution for a sustainable future by providing a clean and efficient energy carrier [4]. Hydrogen can supply or store energy. Furthermore, it has a very high energy content (i.e. 120 MJ/kg) and can be used in fuel cells (FCs) to generate electricity or power and heat as byproducts. Although hydrogen is not naturally present in nature, it can be found in fossil fuels, biomass, and water. At the present time, hydrogen can be produced in many ways such as by thermochemical, electrolytic, direct solar water splitting, and biological processes [5]. Among these different hydrogen production processes, water electrolysis is a promising option. The operation of water electrolysis is mainly based on the use of electricity to split de-ionized, pure or distilled water into hydrogen and oxygen. The chemical reaction occurs in a system called electrolyzer (EL). On one hand, given that electricity is needed to start hydrogen production, different energy sources can be used. On the other hand, in order to drastically minimize environmental impact, the use of renewable energy sources (e.g. wind, solar) is mandatory [6]. Besides, over the last years, wind energy has gained a growing interest in hydrogen production, as demonstrated in the literature [7]-[14]. In particular, micro-wind energy conversion systems (μWECSs), involving power levels under 10 kW, are attractive for their low cost and easy installation.

Different types of ELs can be distinguished by their electrolyte and the charge carrier: (1) alkaline ELs; (2) proton exchange membrane (PEM) ELs; and (3) solid oxide (SO) ELs [15],[16]. Table I indicates the main features of each technology; whereas Table II presents the advantages and disadvantages of each technology. From Tables I and II, alkaline and PEM ELs are currently the two main technologies, which are commercially available. Alkaline ELs are the most mature and widespread compared to PEM ELs (under development). As highlighted in Table II, alkaline ELs have a longer lifespan than PEM ELs. However, PEM ELs have several advantages over alkaline ELs, such as compactness, fast system response, wide partial load range and high flexibility in terms of operation. As a result, this technology is an attractive option for integration into the grid including renewable power generating systems [16]. For this reason, a PEM EL has been considered for carrying on this work.

Like for FCs, DC/DC converters are mandatory to interface the DC voltage grid and the EL. Generally, the EL required a very low DC voltage in order to generate hydrogen. Indeed, at nominal power, the cell voltage of an EL is equal around to 2.5 V [17]. With the aim to optimize the reliability of the EL, the number of cells has to be limited. As emphasized in a previous work [17], DC/DC converters for EL applications must meet several requirements from voltage ratio, energy efficiency, and low output current ripple point of view. Among these issues, the most important requirement expected from the DC/DC converter is a high conversion ratio. Indeed, for hydrogen production via water electrolysis from WECSs, the DC bus voltage is very high (i.e. between a hundred and a thousand volts) [17]. Given that the voltage of the electrolyzer is quite low (i.e. around ten volts) [17], DC/DC converters for EL applications must have a high conversion ratio ability.

Based on the current literature survey carried out in a previous work [17], three types of DC/DC converters are mainly used for these applications: (1) buck converter; (2) half-bridge converter (HBC); and (3) full-bridge converter (FBC). On one hand, classic buck converters are widely used within hydrogen production systems based on WECS [7]-[14]. In [7], Şahin et al. have proposed a synchronous buck converter by replacing the diode with a power switch. Therefore, the diode reverse recovery issue can be removed. In the other related papers [8-14], a simple buck converter is used since the study is mainly focused on energy management and cost analysis. By comparison, in [18], Monroy-Morales proposes a system composed of a rectifier and a classic buck converter to supply an electrolyzer. The rectifier is used to convert an AC grid to a DC grid; whereas the buck converter is used to adjust the required voltage to supply the electrolyzer. On the other hand, classic buck converters present several disadvantages,

particularly from voltage ratio and output current ripples reduction point of view. These topologies must be particularly used for applications requiring a low voltage ratio as reported in the literature (i.e. for very small, low voltage wind turbines) [7]-[14]. On the other side, isolated DC/DC converter topologies (e.g. HBC, FBC) provide more perspective, especially in terms of voltage conversion ratio due to the use of a transformer. In [19],[20], Andrijanovitš et al. have developed a zero-voltage switching half-bridge DC-DC converter to interface the DC grid and the electrolyzer within a stand-alone power supply based on renewable energy sources. By comparison, in [21], Blinov and Andrijanovitš have developed a half-bridge phase-shifted active rectifier for electrolyzer applications. Finally, full-bridge DC-DC converters have been proposed in [22-28]. The advantages and disadvantages of each topology have been provided in a previous review work [17]. If the transformer is well designed for a given application, these topologies are particularly suitable for hydrogen production via water electrolysis including WECS. However, so far, they have not been considered in the literature for these applications [17].

Accordingly, the main purpose of this paper is to present a suitable-high voltage ratio DC/DC converter for EL applications within a hydrogen production system based on a WECS. In this application, the DC bus voltage is quite high (i.e. around a hundred volts) and is very representative of the usual DC bus grid voltage met in wind power systems; consequently, a DC/DC converter with high conversion ratio is required. Another important aspect treated in the paper is the control of the DC/DC converter. In this paper, model-based control techniques are used. To this end, a mathematical model is obtained, assuming the behavior of the transformer as ideal. Using this model, two controllers are designed, one consisting of integral action, and the other consisting of an integral action together with a proportional action. Experimental tests have been carried out in order to validate the concept of the developed converter and its control for applications requiring a high conversion ratio.

This paper is divided into five sections. After this Introduction presenting the current state-of-the-art and motivations to carry out this work, Section 2 describes the investigated hydrogen production system (i.e. from the wind turbine to the EL), and particular attention is given to the proposed DC/DC converter. Then, in Section 3, details about the design and control laws for the DC/DC converter are provided. Finally, Section 4 presents the experimental test bench used to validate the proposed DC/DC converter and its control, as well as the obtained results.

## 2. THE INVESTIGATED SYSTEM AND THE CHOSEN CONVERTER TOPOLOGY

Within the framework of this work, a hydrogen production system based on a μWECS is investigated and is shown in Fig. 1. This system is composed of the following components: a horizontal axis wind turbine, a three-phase bridge rectifier, the proposed DC/DC converter, and finally a PEM electrolyzer and metal-hydride hydrogen storage. In the following, further details are provided for each component being part of the studied hydrogen production system.

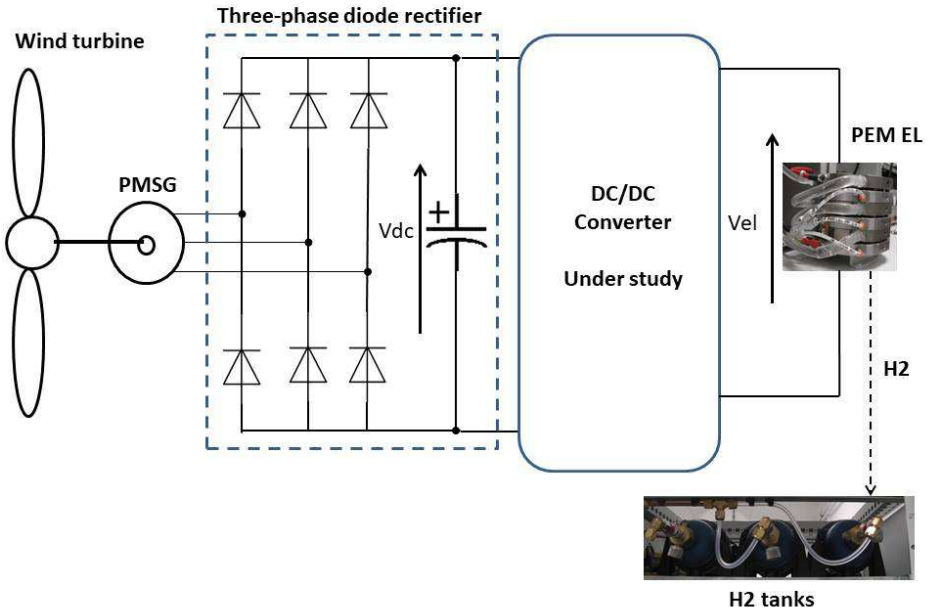


Figure 1: Synopsis of the investigated hydrogen production system.

### 2.1. Wind turbine

In this work, the features of a horizontal axis three-phase wind turbine manufactured by FORTIS company were used. The wind turbine consists of the following parts: frame/generator/mast adapter; rotor blades/hub and finally a tail with the tail vane. The technical data of the wind turbine are provided in Table III. The wind turbine is located on the campus of the IUT (i.e. University of Technology) in Longwy (France), a section of the University of Lorraine. The trend of turbine power with wind speed is provided in Fig. 2.

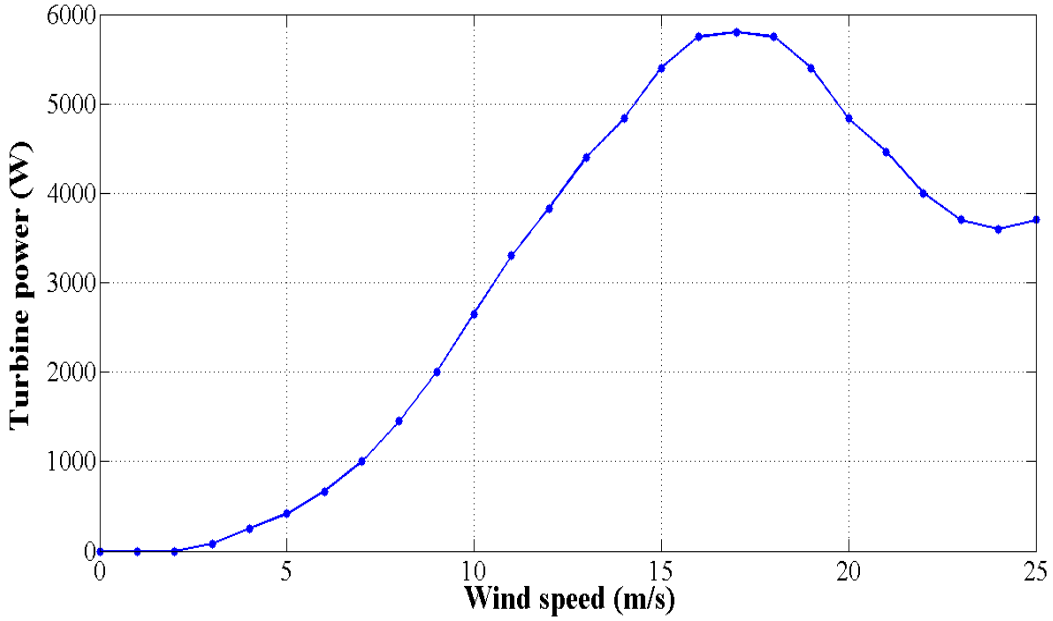


Figure 2: Power curve of the wind turbine according to the wind speed.

## 2.2. PMSG and Three-phase diode rectifier

The FORTIS wind turbine is connected to a brushless permanent magnet synchronous generator (PMSG), that outputs a three-phase AC voltage, whose frequency and amplitude depend on wind speed. The PMSG output is connected to a three-phase diode rectifier and a capacitive filter to obtain a DC voltage. The variation of the DC voltage with wind speed is provided in Fig. 3. According to this figure, the DC bus voltage range is from 75 V (cut in wind speed) to 500 V (rated wind speed).

Based on the wind speed measurements carried out on the campus, the considered wind speed range is from 5 to 7 $m.s^{-1}$. As a result, the DC bus voltage at the output of the rectifier is comprised between 150 V and 220 V.

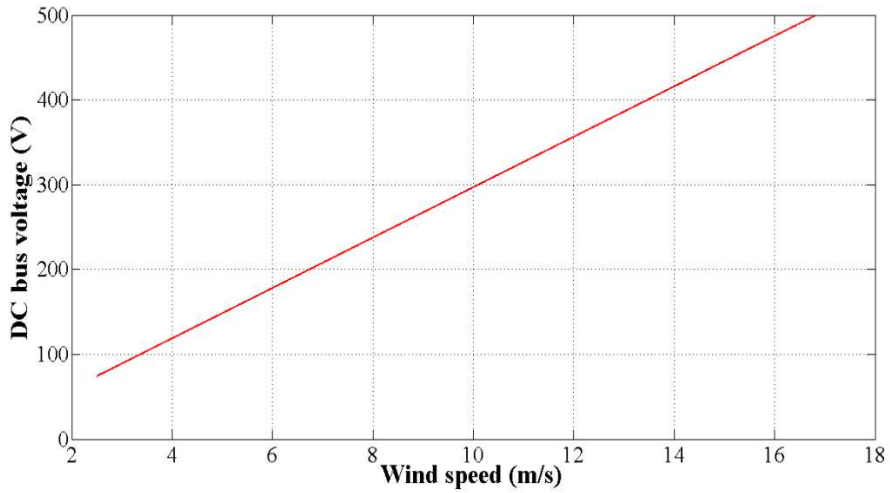


Figure 3: Variation of DC bus voltage at the output of the rectifier according to wind speed.

## 2.3. Electrolyzer and hydrogen storage

A PEM EL (NMH2 1000) from the HELIOCENTRIS company is connected to the developed DC/DC converter. The features of the PEM EL are provided in Table IV. The operating principle of this EL is shown in Fig. 4. The generated hydrogen gas is accumulated in the hydrogen/water separator and is dried by passing through the automatic dryer. The internal pressure (11 bar) is controlled by the amount of generated hydrogen by the cell. The output pressure is controlled by a proportional valve.

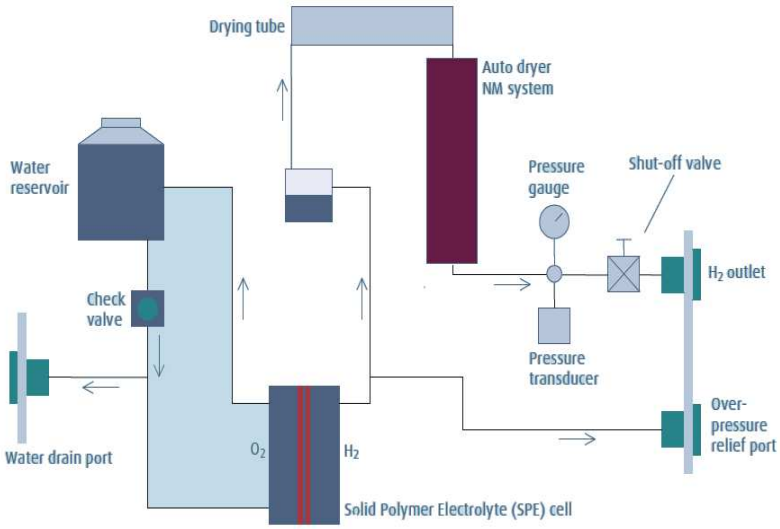


Figure 4: Operating principle of the PEM EL.

In order to store hydrogen produced by the PEM EL, three metal hydride storage systems (MHS 800 shown in Fig. 1) from the HELIOCENTRIS company are used. These tanks are equipped with a low-temperature metal alloy on a titanium (Ti) and magnesium (Mg) base. They present several benefits for storage as defined below:

- Absorption of the hydrogen in the alloy lattice after the adsorption at the surface;
- can store hydrogen at high volume and low weight density (fit for stationary applications);
- low thermal conductivity.

The technical data of the MHS 800 metal hydride storage are provided in Table V.

## 2.4. Proposed and developed DC/DC converter

In the proposed application, the electrolyzer is supplied by a wind turbine connected to a PMSG and, in turn, to a three-phase bridge rectifier (Fig. 1). On the one hand, in the operating range, the voltage at the output of the three-

phase diode rectifier (DC bus voltage) varies from 150 V to 220 V. On the other hand, the electrolyzer requires a rated power of 400 W with a voltage of 8 V. Therefore, a step-down DC/DC converter is required. Unfortunately, such a strong voltage reduction cannot be obtained with a traditional single-stage buck converter since a very low duty cycle (ranging between 0.036 and 0.053) would be necessary; in such case, the low conduction time of the power switch would require a very fast on and off time of the device, and the current supplied by the source would have a high di/dt. Moreover, at constant input-output power, a strong voltage reduction implies a very high value of the output current; thus, the inductor, the power switch, and the free-wheeling diode would be subjected to high current levels degrading the efficiency due to Joule losses. The second disadvantage could be partially solved by an interleaved step-down converter in which the current is shared among more inductors [7]. As a matter of fact, this circuit operates as more parallel connected converters and the total current is divided. Hence, the current ratings of power electronics devices could be reduced. Anyway, to assure that all currents are equally divided among inductors, and to properly control and improve the reliability of interleaved topologies, several current sensors must be used [29],[30]. However, the more current sensors are used, the more the control is complex. Anyway, the classic interleaved step-down converter does not help to solve the first disadvantage (i.e., the need for very fast devices and the related high di/dt) because it still has a limited voltage ratio.

For the above-mentioned reasons, a different topology has been chosen for the proposed DC/DC converter. The synopsis of the chosen topology is shown in Fig. 5; it encompasses a buck converter stage connected to an FBC, operating at a constant duty cycle, a transformer (2) with a suitable reduction ratio, a bridge rectifier (3), an LC filter (4). Further details regarding the design of the converter are provided in Section 3. In the following, the reasons that led to choosing this topology will be explained. A strong voltage reduction can be obtained easily only by using a transformer with a suitable voltage ratio. The working frequency of such a component is chosen as a compromise: a value lower than 100 Hz implies a heavy and bulky transformer; on the other hand, significant switching losses are exhibited when the frequency exceeds 50 kHz. Therefore, a working frequency of 25 kHz has been chosen for the transformer. Being the transformer an AC device, an FBC is required to convert the rectified DC wind turbine voltage into a 25 kHz square wave that is fed into the high side of the transformer (high voltage, low current). In addition, a classic buck converter is placed between the three-phase rectifier and the input of the FBC to have one degree of freedom (i.e., the control variable) on the voltage/current combination at each power level. The higher

current appearing at the low side of the transformer is simply rectified using a diode bridge. Finally, a low-pass LC filter reduces the current and voltage ripple to extend the life of the EL. The present study focuses specifically on ELs supplied by μWECS, i.e., with power levels lower than 10 kW. As for the high-side section of the circuit, in the chosen case study a maximum current of 1.8 A is obtained at the considered power and voltage levels (400 W and 220V); in the worst case (i.e., for a typical 10 kW, 400 V three-phase wind turbine), the current is lower than 15 A. Hence, the choice of the classic buck converter placed between the three-phase rectifier and the input of the FBC is adequate, and no current sharing is required. Specifically, the buck converter is used to obtain a moderate voltage reduction ratio, which is then further increased by the transformer. As for the low-side section of the circuit, in the chosen case study a maximum current of 50 A is obtained at the considered power and voltage levels (400 W and 8 V); in the worst case (i.e., for a 10 kW wind turbine), the current is 1250 A. However, these higher current levels are not a problem since the related circuit is completely passive (i.e., diodes are used instead of active switching devices). Even if several parallel-connected diodes are used, being the circuit passive no current sharing issues arise. Therefore, all the electric components required by the proposed topology are readily available on the market (diodes) or can be simply designed and built (high-frequency transformers with high secondary current). It is worth noting that, for power levels higher than 10 kW, alternative DC/DC converter topologies may be more suitable, but the analysis of this scenario falls outside the scope of the present paper.

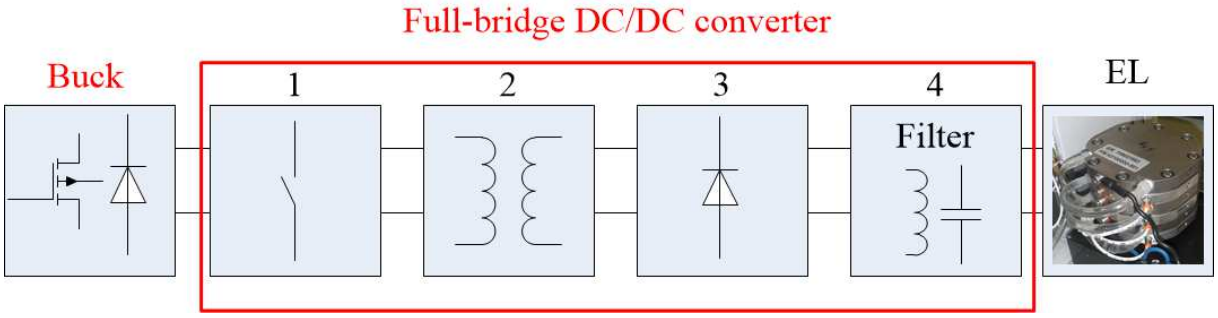


Figure 5: Synopsis of the proposed DC/DC converter.

## 3. CONVERTER DESIGN AND DEVELOPMENT OF THE CONTROL LAWS

### 3.1. Design and sizing of the proposed converter

In general, it is possible to size the output filter of the FBC ((4) in Fig. 4) considering that the output waveforms of an FBC with unity turn ratio, controlled with duty ratio D at a switching frequency $F_{sw}$, are the same as those of a

buck converter operating at 2D and $2F_{sw}$ [31]. In the case under study, the FBC is operated at a constant duty ratio equal to 0.5. As a result, the output waveforms should have no ripples at all. However, the leakage inductance of the high-frequency transformer (HFT) and the inductance of the output filter of the FBC significantly delay the commutation between the diode paths corresponding to a positive and negative current, and the voltage at the secondary side of the HFT is zero during the commutation. Hence, the actual duty ratio of the equivalent buck converter is lower than unity and not constant. Two SEMISTACK-IGBT from SEMIKRON company will be used for implementing the proposed converter, as discussed in Section 4; hence, no sizing is required for IGBTs and diodes. On the other hand, the different passive components to design for our system are shown in Fig. 6. Actually, there are 6 passive components to design (3 inductors, 3 capacitors): one LC couple at the output of the buck converter, and two LC couples both at the input and the output of the full-bridge DC-DC converter.

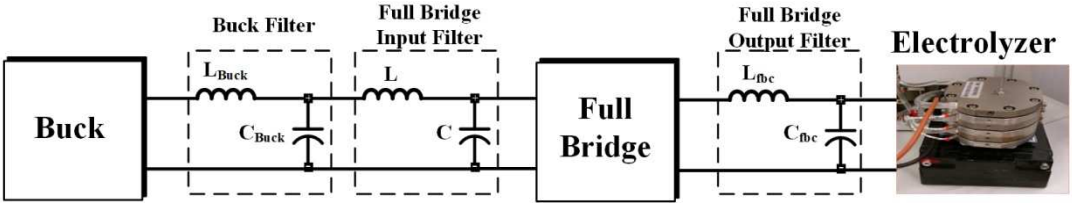


Figure 6: Overview of passive components to design.

The HFT aims at reducing the voltage from about 80 V to about 8 V (EL rated voltage) and increasing the current from 5 A to 50 A. Therefore, a turn ratio equal to N=10 is required. The HFT has been built on purpose and exhibits a magnetizing inductance of 0.4 mH, a leakage inductance of 24 µH, and parasitic resistance of 5.4 mΩ. The inductor of the output filter is sized imposing an output current ripple of 1% in the worst case (i.e. when the equivalent buck converter is controlled with a duty cycle equal to D=0.5). Taking the turn ratio of the HFT into account, we obtain the minimum value for such an inductor [31]:

$$L_{FBC} = \frac{V_{in}/K}{8 \cdot 2F_{sw} \cdot I_{out,max} \cdot r_i/100} = 50\ \mu H \quad (1)$$

The chosen commercial inductor has an inductance of 50 µH and parasitic resistance of 4.5 mΩ.

As for the output capacitor, it is designed to obtain a voltage ripple ($r_v$) of 1% in the worst case (i.e. with a low duty ratio). Considering D=0.165 for the HFB (i.e. D=0.33 for the buck converter), the maximum corner frequency $f_{c,max}$ of the low pass filter can be determined as follows [31]:

$$\frac{\Delta V_{out}}{V_{out}} = \frac{2r_v}{100} = \frac{\pi^2}{2}(1-2D)\left(\frac{f_c}{2F_{sw}}\right)^2 \quad (2)$$

$$f_{c,max} = 2F_{sw}\sqrt{\frac{2r_v}{100}\cdot\frac{2}{\pi^2}\cdot\frac{1}{1-2D}} = 3112\ Hz \quad (3)$$

Therefore, the required minimum capacitance value is:

$$C_{FBC,min} = \frac{1}{L_3}\left(\frac{1}{2\pi f_{c,max}}\right)^2 = 53\ \mu F \quad (4)$$

The chosen commercial capacitor has a capacitance of 56 µF and parasitic resistance of 28 mΩ.

The input current of the FBC has a large and spiky ripple superimposed on the DC component. If this ripple is handled only by a capacitor, the required capacitance value is 10 mF. However, this choice would lead up to very slow dynamics of the converter. Hence, an LC filter is preferred as the input filter of the FBC. The related components will be chosen after sizing the passive components of the input buck converter. This converter aims at reducing the rectified output of the wind generator (about 200 V, 400 W) to the voltage and current levels required at the input of the FBC. Due to the non-ideal commutation and reduced equivalent duty ratio, the input voltage must be slightly higher than 80 V; actually, 92.5 V and 4.32 A are required at the input of the FBC (i.e. at the output of the buck converter). Using the usual formulas for sizing the output inductor of the buck converter [31] and imposing a current ripple of 25% in the worst case, we obtain:

$$L_{buck,min} = \frac{V_{in}}{8\cdot F_{sw}\cdot I_{out,max}\cdot r_i/100} = 1.16\ mH \quad (5)$$

The chosen commercial inductor has an inductance of 1.2 mH and parasitic resistance of 33.33 mΩ.

As for the output capacitor, it is designed to obtain a voltage ripple of 1%. Considering D=92.5/200=0.4625, the maximum corner frequency $f_{c,max}$ of the low pass filter can be determined as follows [31]:

$$f_{c,max} = F_{sw}\sqrt{\frac{2r_v}{100}\cdot\frac{2}{\pi^2}\cdot\frac{1}{1-D}} = 1737\ Hz \quad (6)$$

Therefore, the required minimum capacitance value is:

$$C_{buck,min} = \frac{1}{L_1}\left(\frac{1}{2\pi f_{c,max}}\right)^2 = 7\ \mu F \quad (7)$$

The chosen commercial capacitor has a capacitance of 20 µF and parasitic resistance of 16 mΩ. The corner frequency of the obtained LC low-pass filter is 1027 Hz. The subsequent LC low-pass filter (i.e. the input filter of the FBC) is designed to have a slightly lower corner frequency (735 Hz) and a sufficiently large input impedance compared to the output impedance of the preceding LC filter (0.4 Ω). Consequently, the chosen commercial

inductance and capacitance values are 100 µH and 470 µF, respectively. The related parasitic resistances are 9 mΩ and 110 mΩ, respectively. In Fig. 6, these two passive components are named L and C.

### 3.2. Control laws for the proposed DC/DC converter

a) Mathematical model

The electrical scheme of the overall system is shown in Fig. 7, where the buck converter drives a full-bridge whose output is connected to the primary of a transformer; the secondary of the transformer supplies the EL through a rectifier and an LC filter. The electrolyzer is physically modeled by means of resistance, $R_{elec}$, and a DC generator, $E_{elec}$, series connected.

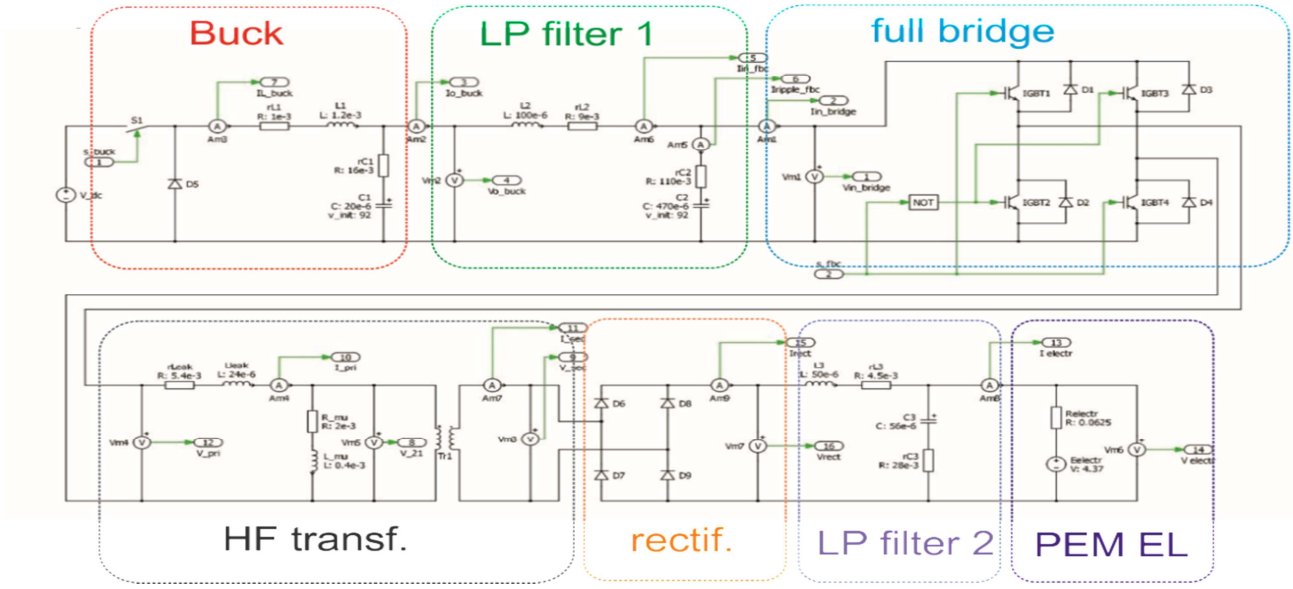


Figure 7: Physical model of the set controlled buck, full-bridge, transformer, rectifier, and electrolyzer.

The inductors $L_1$ and $L_2$ are physically modeled as inductances, $L_1$ and $L_2$, connected in series to parasitic resistances $r_{L1}$ and $r_{L2}$, respectively. The capacitors, $C_1$ and $C_2$ are modeled as capacitances, $C_1$ and $C_2$, connected to parasitic resistances, $r_{C1}$ and $r_{C2}$, respectively, connected in series to them.

The voltage $V_{DC}$ is the DC bus voltage at the output of the three-phase rectifier (see Fig. 1), assumed equal to 200 V, which represents the input of the buck converter. The output of the latter supplies the full-bridge which operates at a duty cycle of 50% and produces an alternate voltage. Such a waveform is applied to the transformer, whose output is, firstly, rectified and then applied to the electrolyzer through the filter $L_3$-$C_3$. The parasitic resistances of this filter are neglected. The transformer will be assumed ideal for the development of the mathematical model, whereas for

simulation its leakage inductance and resistance and magnetization inductance and resistance will be included in the physical model.

In these hypotheses, since the full-bridge input voltage, $v_B$, and the corresponding input current $i_B$ are positive whatever the operative conditions, the following useful considerations for modeling the system of Fig. 7 can be made:

1. When the switch $S_1$ is in the ON state and IGBT1 and IGBT4 are in the ON state, the voltage $v_{1t} = v_B$ at the primary of the transformer is positive; the voltage $v_{2t} = Nv_{1t}$ at the secondary is positive too, and consequently the diodes $D_6$ and $D_9$ are ON and then the current $i_{2t} = i_{1t}/N$, where $N$ is the inverse of the turns ratio ($v_{1t}/v_{2t}$).
2. When the switch $S_1$ is in the ON state and IGBT2 and IGBT3 are in the ON state, the voltage $v_{1t} = -v_B$; the voltage $v_{2t} = Nv_{1t}$ at the secondary is negative, and consequently the diodes $D_7$ and $D_8$ are ON and then the current $i_{2t} = i_{1t}/N$.
3. When the switch $S_1$ is in the OFF state and IGBT1 and IGBT4 are in the ON state, the same considerations in 1 hold. It follows that the model is the same of that relative to the operating conditions as in 1, assuming $V_{dc} = 0$.
4. When the switch $S_1$ is in the OFF state and IGBT2 and IGBT3 are in the ON state, the same considerations in 2 hold. It follows that the model is the same of that relative to the operating conditions as in 2.

The above considerations clearly show that the model corresponding to the operation detailed in 1 is valid also in the operations discussed in 2, and in those discussed in 3-4 assuming $V_{dc}$=0.

Regarding the development of the model describing the operation in 1, it is worth noting that the assumption of ideal transformer allows obtaining a linear and time-invariant model in which all the variables are continuous-type, in the sense that the set full-bridge, transformer, and rectifier is crucial for obtaining the desired operations in alternating current (AC), but this set does not contribute to the construction of the model itself.

In order to develop the model of the system depicted in Fig. 7, relative to the condition where $S_1$ is in the ON state, note that the input variables are $V_{dc}$ and $E_{elec}$, the state variables are the currents flowing through the inductances $L_1$, $L_2$ and $L_3$, namely $i$, $i_2$ and $i_o$, respectively, and the voltages on the capacitances $C_1$, $C_2$ and $C_3$, namely $v_{c1}$, $v_{c2}$ and $v_{c3}$. It is assumed that the current $i_o$ flowing through the inductance $L_3$ is the output variable. This current coincides

practically with the input current of the electrolyzer $i_{el}$ and, consequently, current control of the electrolyzer is performed. The use of the current $i_o$ as output simplifies the model of the system together with the control problem, because it is a state variable, maintaining the same objective of controlling the input current of the electrolyzer.

For the operation case detailed in 1, the state-space model of the physical model shown in Fig. 7, from the DC bus voltage $V_{dc}$ at the output of the three-phase rectifier to the electrolyzer, is provided below:

$$\dot{x} = A_{ON}x + B_{ON}u \tag{8}$$

$$y = c_{ON}^T x \tag{9}$$

where $x = [i \quad i_2 \quad v_{c1} \quad v_{c2} \quad i_o \quad v_{c3}]^T$, $u = [V_{dc} \quad E_{elec}]^T$, $y = v_{c3}$,

$$A_{ON} = \begin{bmatrix} -\frac{r_{L1}+r_1}{L} & \frac{r_1}{L} & -\frac{1}{L} & 0 & 0 & 0 \\ \frac{r_1}{L_2} & -\frac{r_1+r_2+r_3}{L_2} & \frac{1}{L_2} & -\frac{1}{L_2} & \frac{Nr_3}{L_2} & 0 \\ \frac{1}{C_1} & -\frac{1}{C_1} & 0 & 0 & 0 & 0 \\ 0 & \frac{1}{C_2} & 0 & 0 & -\frac{N}{C_2} & 0 \\ 0 & \frac{Nr_3}{L_3} & 0 & \frac{N}{L_3} & -\frac{N^2r_3}{L_3} & -\frac{1}{L_3} \\ 0 & 0 & 0 & 0 & \frac{1}{C_3} & -\frac{1}{R_1C_3} \end{bmatrix}, B_{ON} = \begin{bmatrix} \frac{1}{L} & 0 \\ 0 & 0 \\ 0 & 0 \\ 0 & 0 \\ 0 & 0 \\ 0 & \frac{1}{R_1C_3} \end{bmatrix}$$

$$c_{ON}^T = [0 \quad 0 \quad 0 \quad 0 \quad 1 \quad 0].$$

The model corresponding to $S_1$ in the OFF state, is given by:

$$\dot{x} = A_{OFF}x + B_{OFF}u \tag{10}$$

$$y = c_{OFF}^T x \tag{11}$$

where $A_{OFF} = A_{ON}$, $c_{OFF}^T = c_{ON}^T$, and:

$$B_{OFF} = \begin{bmatrix} 0 & 0 \\ 0 & 0 \\ 0 & 0 \\ 0 & 0 \\ 0 & 0 \\ 0 & \frac{1}{R_1C_3} \end{bmatrix}.$$

Starting from the developed models (8)-(9) and (10)-(11), and assuming that the buck operates in continuous conduction mode, the average state space model is given by:

$$\dot{x} = Ax + Bu \tag{12}$$

$$y = c^T x \tag{13}$$

where:

$$A = A_{OFF} + (A_{ON} - A_{OFF})d = A_{OFF}$$

$$c^T = c_{OFF}^T + (c_{ON}^T - c_{OFF}^T)d = c_{OFF}^T$$

In which $d$ is the duty cycle (i.e. the control input of the whole system). With these definitions, equation (12) can be put under this form:

$$\dot{x} = Ax + B_{OFF}u + (B_{ON} - B_{OFF})ud \tag{14}$$

In order to bring back again the model (14) in the standard form, we define the equilibrium state of the model (14), corresponding to the constant input $u$ and a duty-cycle $d^*$, as the state $x^*$ which satisfies the equation:

$$0 = Ax^* + B_{OFF}u + (B_{ON} - B_{OFF})ud^*$$

This state surely exists since the matrix $A$ is invertible and it is given by:

$$x^* = A^{-1}[B_{OFF}u + (B_{ON} - B_{OFF})ud^*] \tag{15}$$

Denoting by $\tilde{x} = x - x^*$ the state variable relative to the equilibrium state, the model of the system can be put under the standard form:

$$\dot{\tilde{x}} = A\tilde{x} + b\tilde{d} \tag{16}$$

$$\tilde{y} = c^T\tilde{x} \tag{17}$$

in which $\tilde{d}$ is the control variable, $b = (B_{ON} - B_{OFF})u$ and $\tilde{y}$ is the output relative to the equilibrium output $c^T x^*$.

b) Controller design

The electrolyzer current to duty cycle transfer function of model (16)-(17) is given by:

$$G_p = \frac{\widetilde{i_{el}}}{\tilde{d}} = c^T(sI - A)^{-1}b = K_p \frac{(s-z_1)(s-z_2)(s-z_3)}{(s-p_1)(s-p_2)(s-p_3)(s-p_4)(s-p_5)(s-p_6)} \tag{18}$$

where:

$$K_p = 4.85 \times 10^9,\ z_1 = -3.125 \times 10^6,\ z_2 = -1.193 \times 10^4,\ z_3 = -2.857 \times 10^5,$$
$$p_1 = -2.845 \times 10^5,\quad p_2 = -640 - j23680,\ p_3 = -640 + j23680,\ p_4 = -1147,$$
$$p_5 = -104 - j1311,\ p_6 = -104 + j1311$$

As it can be observed, $z_3 \cong p_1$ and, consequently, there is a pole-zero cancellation in the transfer function $G_p$. It follows that the model is not controllable and observable at the same time. Instead, it can be easily verified that it is controllable, but not observable from the chosen output. However, it is known that the canceled pole is on the left half plane of the Laplace domain.

The bode diagrams of $G_p(j\omega)$ are given in Fig. 8. An analysis of these diagrams shows that the closed-loop system, realized with the transfer function $G_p(s)$ as an open-loop transfer function and unitary feedback, is unstable.

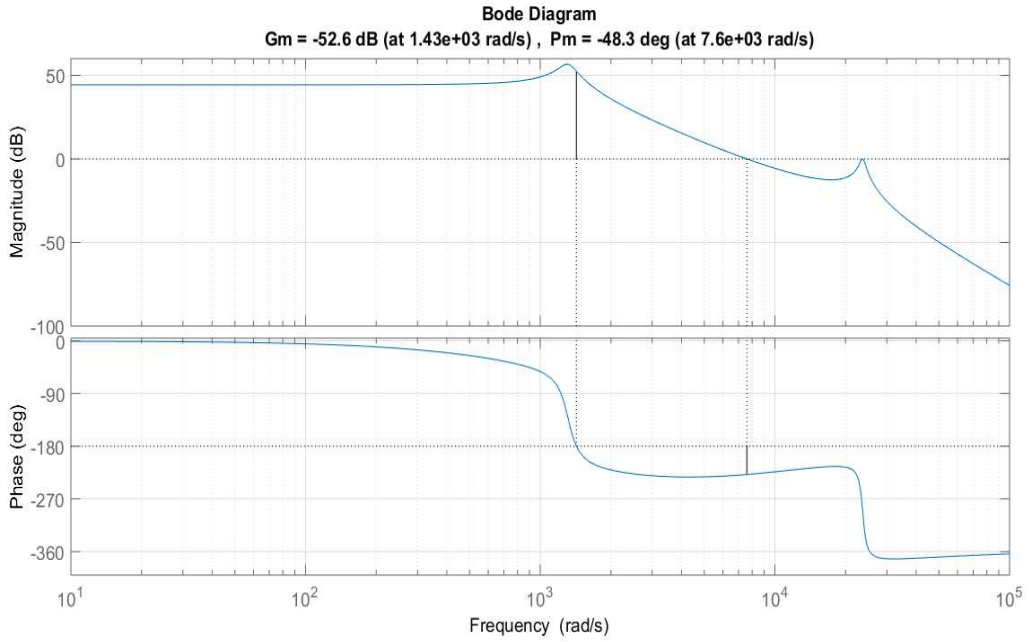


Figure 8: Bode diagram of Gp (jω).

Then, a controller has to be designed so that the closed loop system is stable and satisfies the following additional design requirements:

1. Bandwidth: $B \geq 20$ Hz,
2. Type of the system: 1,
3. Phase margin: $m_{\varphi} \geq 60°$,
4. Attenuation at 1310 rad/s (first resonance frequency): $A_{tn} \geq 10$ dB,
5. Gain margin: $m_g \geq 6$ dB.

With the aim to design the above controller, control theory is applied [31],[32]. First of all, an integral control $G_I(s)=K_{i1}/s$ is added to the plant $G_p(s)$, obtaining the following open-loop transfer function:

$$G_i(s) = K_{i1}\, G_p(s)/s \tag{19}$$

where a gain $K_{i1} = 0.62$ is chosen in order to obtain a crossover frequency of 100 rad/s. The Bode diagrams of the open-loop transfer function (19) are given in Fig. 9. The closed-loop system is stable and the requirements of gain and phase margins are satisfied.

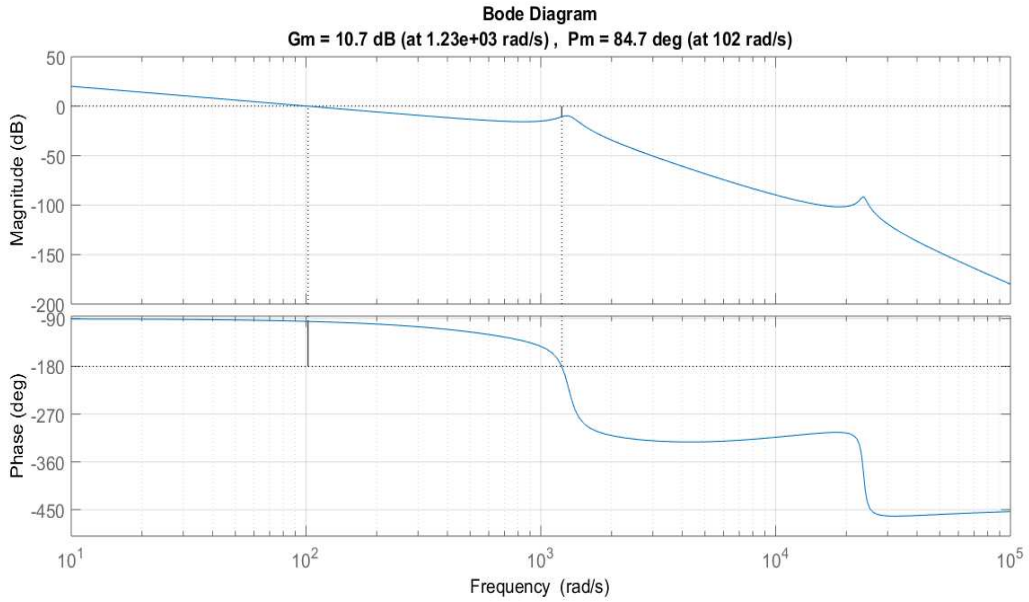


Figure 9: Bode diagrams of function $G_i(j\omega)$.

## 4. EXPERIMENTAL TEST BENCH AND VALIDATION

### 4.1. Developed experimental test bench

In order to validate the high voltage ratio converter and its control, experimental tests have been performed. The experimental test bench set up for this work is shown in Fig. 10. It is composed of an auto-transformer which substitutes the wind generator, a 3-phase diode rectifier combined with a buck converter and LC filters, a full-bridge converter followed by a transformer, a diode bridge rectifier including an LC filter, a PEM EL, a metal-hydride hydrogen storage system, de-ionized water tanks, a DS1104 dSPACE board, an interface board, and finally a computer. The 3-phase rectifier, buck, and full-bridge DC/DC converters have been realized by means of two SEMISTACK-IGBT from SEMIKRON company (as shown in Fig. 10). The control of the buck converter, and consequently of the whole DC/DC converter, is closed-loop (as reported in Section 3), whereas that of the full bridge converter is open-loop (based on a duty cycle of 50%), and both have been first carried out in Matlab/Simulink environment, and then implemented into a DS1104 dSPACE board. The control of the buck converter is based on the measurement of the EL current, which is acquired by a PAC10 current clamp from Chauvin Arnoux company. The PWM gate control signals to control the buck and full-bridge DC/DC converters are generated by the dSPACE board. However, the voltage levels of the generated PWM signals from the dSPACE board, 0-5 V, are not suitable to drive the SEMIKRON driver boards SKHI 22, 0-15 V. For this reason, an interface board is used between the dSPACE

board and the driver boards to convert the control signals (0-5V) to (0-15V). Unlike the first SEMISTACK-IGBT, used as a diode rectifier and buck converter, the interface board is implemented on the second SEMISTACK-IGBT, used as full bridge converter. The system specifications are summarized in Table VI.

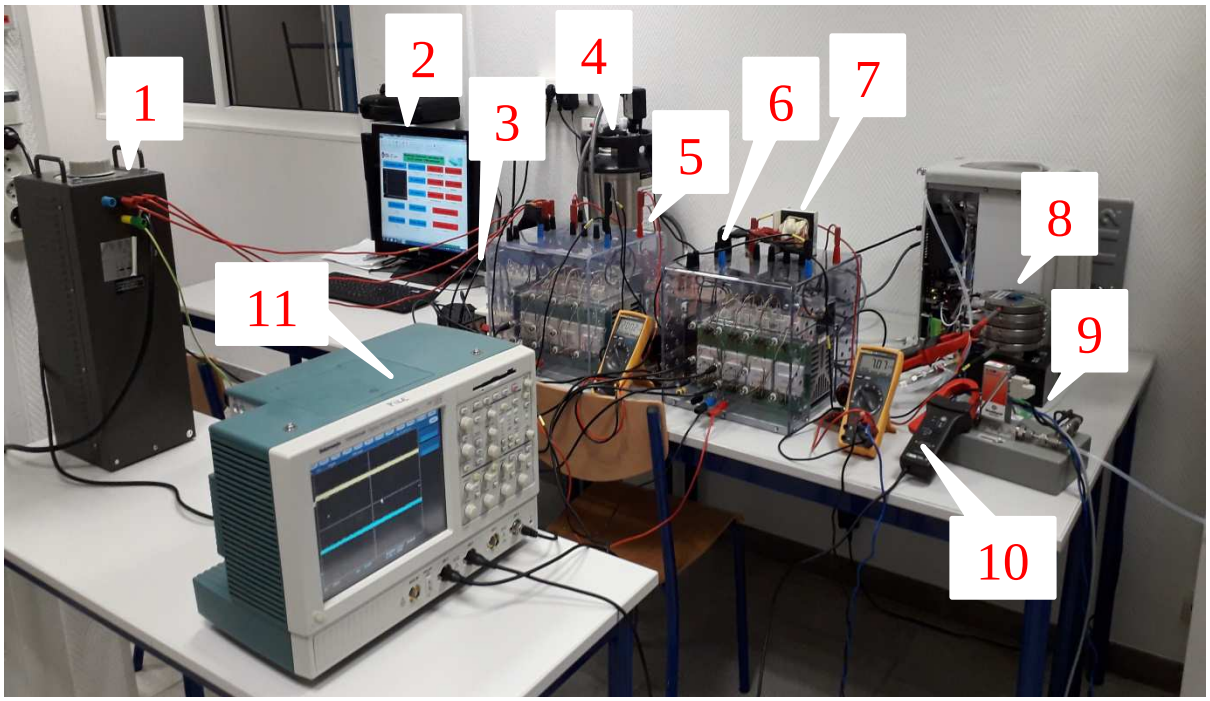


Figure 10: Developed experimental test bench in laboratory: 1) autotransformer (input), 2) dSPACE control desk, 3) dSPACE board, 4) de-ionized water tank, 5) SEMISTACK-IGBT (three-phase diode rectifier and buck converter), 6) SEMISTACK-IGBT (full-bridge converter), 7) high-frequency transformer, 8) proton exchange membrane electrolyzer (output), 9) hydrogen flow rate meter, 10) PAC10 current clamp, 11) 4-channel oscilloscope.

## 4.2. Experimental validation of the developed DC/DC converter and its control

Based on the developed experimental test bench, three closed-loop dynamic tests have been performed by implementing the designed an integral type controller in Matlab/Simulink environment and, subsequently, transferring it into the DS1104 dSPACE board.

The first dynamic test consists in modifying the EL current control (from open-loop to closed loop) for $V_{dc}$=200V; for the second test, the DC bus voltage is modified from 150 V to 200 V while the converter operated in closed-loop. The obtained results are shown in Fig. 11. As it can be observed in Fig. 11a, the designed DC/DC converter, although controlled by an integral type controller based on the EL current, is able to supply the electrolyzer with a good

dynamic performance. Obviously, the static behavior is of type 1. By comparison, in Fig. 11b, the sudden variation of the DC bus voltage leads up to an overshoot of the buck current converter around 6 A. This overshoot has to be as low as possible in order to protect the power switch against high current stress. Besides, the current ripples are higher due to the DC bus voltage increase. Regarding the EL current, a low overshoot can be noticed (around 2 A) before reaching its steady-state operation (around 10 A) quickly.

The steady-state operation of the buck converter and electrolyzer is shown in Fig. 12, in both the above-mentioned experiments, is in the range of continuous conduction mode, with the duty-cycle greater than 0.3. Besides, the EL current ripple is close to zero due to the use of an LC filter between the full-bridge and the EL, whereas the EL voltage is perfectly continuous. Therefore, by minimizing this ripple, the performance of the whole system DC/DC converter-electrolyzer has been enhanced.

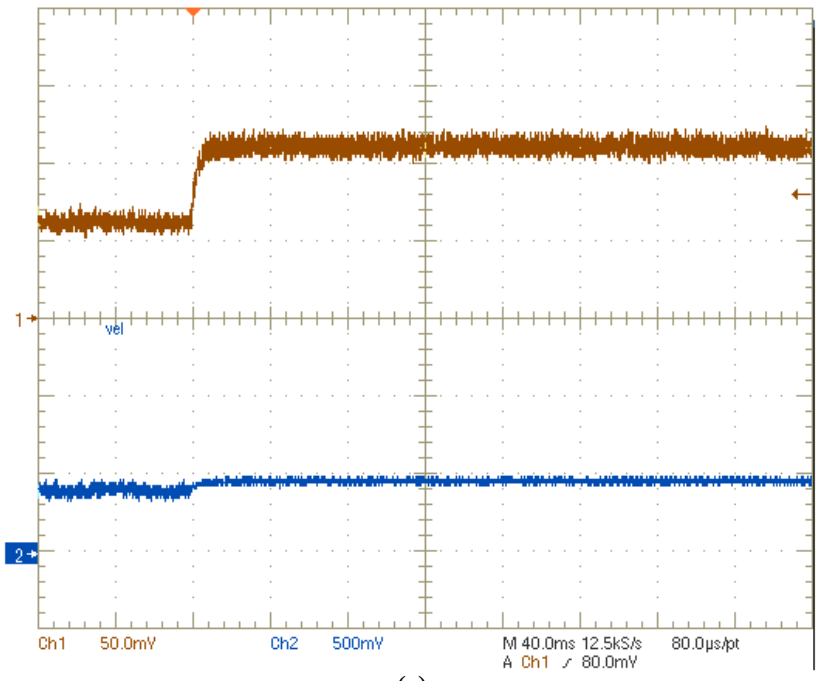


(a)

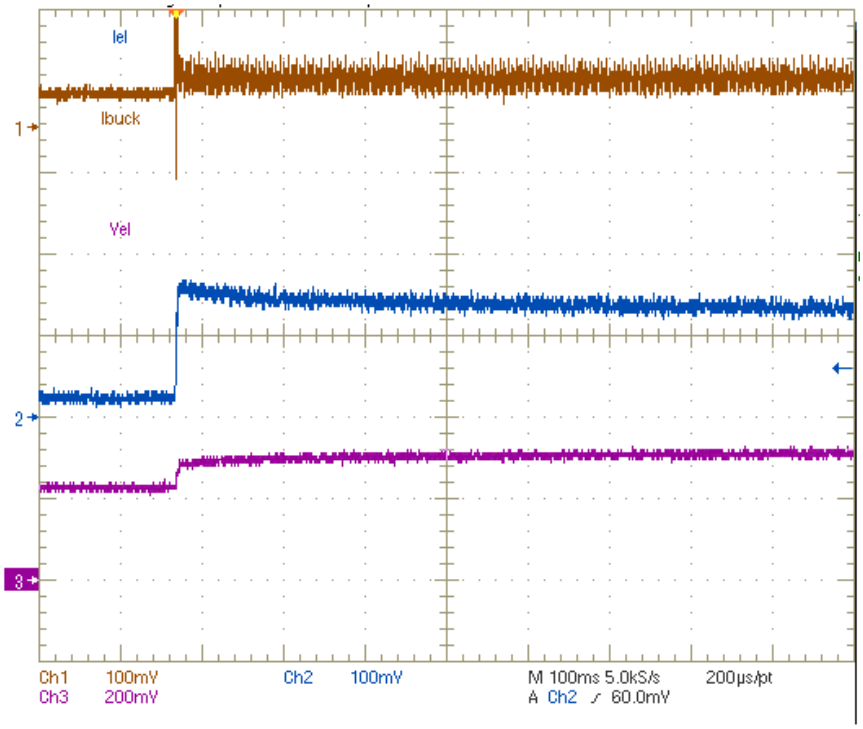


(b)

Figure 11: (a) first dynamic test, channel 1: buck current (5 A.div–1), channel 2: EL voltage (10 V.div–1). (b) second dynamic test channel 1: buck current (10 A.div–1), channel 2: EL current (10 A.div–1), channel 3: EL voltage (4 V.div–1).

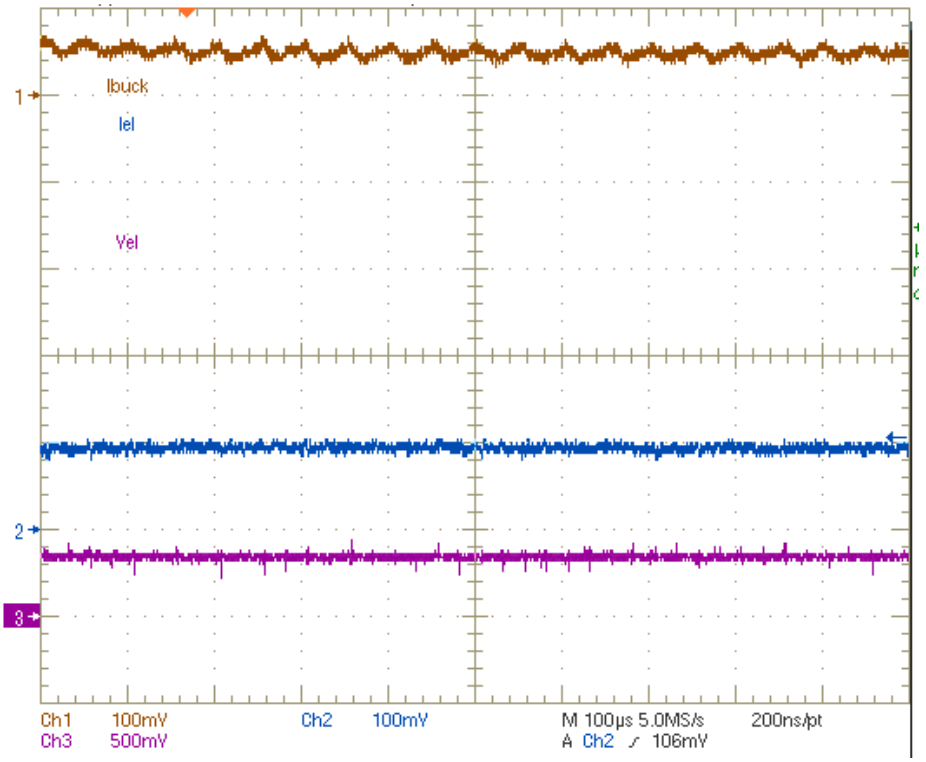


Figure 12: Steady-state operation, channel 1: buck current (10 A.div–1), channel 2: EL current (10 A.div–1), channel 3: EL voltage (10 V.div–1).

## 5. CONCLUSION

The main objectives of the work were to design and develop a high-voltage ratio DC/DC converter based on buck and full-bridge DC/DC converters. Indeed, based on the current literature, it was demonstrated that current hybrid renewable energy systems with a hydrogen buffer storage are limited to low-power applications. This can be explained by the use of classical DC/DC converters (buck converters for electrolyzer applications) which present several drawbacks from voltage ratio and output current ripple points of view. Therefore, in order to move towards medium and high-power applications, DC/DC converters must feature high conversion ratio ability.

The design of the whole system including the different filters has been carried out with the aim to minimize the output current ripple Besides, the control has been developed to ensure good dynamic performances in case of sudden variations of the operating conditions. Experimental tests have allowed validating the proposed high-voltage ratio converter and the control as well. The obtained experimental results demonstrate the good performances from steady-state error and stability points of view. Furthermore, the current ripple at the input of the electrolyzer is close to zero, as expected, and allows optimizing the

electrolyzer performance from efficiency and hydrogen production points of view. Future works will be carried out in order to develop other robust controls with the aim to enhance the performance of the proton exchange membrane electrolyzer.

## REFERENCES

[1] M. Höök, X. Tang, Depletion of fossil fuels and anthropogenic climate change-A review, Energy Policy 52 (2013) 797-809.

[2] Ipcc.ch. (2019). AR6 Climate Change 2021: Impacts, Adaptation and Vulnerability — IPCC. [online] Available at: https://www.ipcc.ch/report/sixth-assessment-report-working-group-ii/.

[3] Bp.com. (2019). [online] Available at: https://www.bp.com/content/dam/bp/business-sites/en/global/corporate/pdfs/energy-economics/statistical-review/bp-stats-review-2018-full-report.pdf.

[4] E. Zoulias, E. Varkaraki, N. Lymberopoulos, C.N. Christodoulou, G.N. Karagiorgis, A review on water electrolysis, TCJST 4 (2) (2003) 41-71.

[5] Hydrogen.energy.gov. (2019). DOE Hydrogen and Fuel Cells Program: 2017 Annual Merit Review Proceedings. [online] Available at: https://www.hydrogen.energy.gov/annual_review17_proceedings.html.

[6] N.L. Panwar, S.C. Kaushik, S. Kothari, Role of renewable energy sources in environmental protection: A review, Renewable and Sustainable Energy Reviews 15 (3) (2011) 1513-1524.

[7] M.E. Şahin, H.I. Okumuş, M.T. Aydemir, Implementation of an electrolysis system with DC/DC synchronous buck converter, International Journal of Hydrogen Energy 39 (2014) 6802-6812.

[8] R. Sarrias-Mena, L.M. Fernández-Ramírez, C.A. García-Vásquez, F. Jurado, Electrolyzer models for hydrogen production from wind energy systems, International Journal of Hydrogen Energy 40 (7) (2015) 2927-2938.

[9] T. Zhou, D. Lu, H. Fakham, B. François, Power flow control in different time scales for a wind/hydrogen/super-capacitors based active hybrid power system, in: Proceedings of 13th IEEE International Power Electronics and Motion Control Conference (EPE/PEMC) (2008) 2205-2210.

[10] T. Zhou, B. François, M. El Hadi Lebbal, S. Lecoeuche, Real-Time Emulation of a Hydrogen-Production Process for Assessment of an Active Wind-Energy Conversion System, IEEE Transactions on Industrial Electronics 56 (3) (2009) 737-746.

[11] J.M. Jacobs, DC/DC Converter for a Small Scale Wind Hydrogen System, Master of Science Thesis, Faculty of the Graduate College, University of Nebraska (2010) 1-73.

[12] T. Zhou, B. François, Modeling and control design of hydrogen production process for an active hydrogen/wind hybrid power system, International Journal of Hydrogen Energy 34 (2009) 21-30.

[13] S.M. Muyeen, R. Takahashi, J. Tamura, Electrolyzer switching strategy for hydrogen generation from variable speed wind generator, Electric Power Systems Research 81 (5) (2011) 1171-1179.

[14] G. Genç, M. Çelik, M. Serdar Genç, Cost analysis of wind-electrolyzer-fuel cell system for energy demand in Pinarbaşi-Kayseri, International Journal of Hydrogen Energy 37 (17) (2012) 12158-12166.

[15] J. Koponen, Review of water electrolysis technologies and design of renewable hydrogen production systems, Master's Thesis, Lappeen University of Technology (2015) 1-87.

[16] Iea.org. (2019). [online] available at: https://www.iea.org/publications/freepublications/publication/TechnologyRoadmapHydrogenandFuelCells.pdf.

[17] D. Guilbert, S.M. Collura, A. Scipioni, DC/DC converter topologies for electrolyzers: state-of-the-art and remaining key issues, International Journal of Hydrogen Energy 42 (38) (2017) 23966-23985.

[18] J.L. Monroy-Morales, M. Hernandez-Angeles, D. Campos-Gaona, R. Pena-Alzola, M. Ordonez, W. Merida, Modeling and control design of a Vienna rectifier based electrolyzer, in: Proc. Of IEEE 7th International Symposium on Power Electronics for Distributed Generation Systems (PEDG) (2016) 1-8.

[19] A. Andrijanovitš, D. Vinnikov, I. Roasto, A. Blinov, Three-Level Half-Bridge ZVS DC/DC Converter for Electrolyzer Integration with Renewable Energy Systems, in: Proceedings of 10th IEEE International Conference on Environment and Electrical Engineering (EEEIC) (2011) 1-4.

[20] A. Andrijanovitš, I. Steiks, J. Zakis, D. Vinnikov, Analysis of State-of-the-Art Converter topologies for Interfacing of Hydrogen Buffer with Renewable Energy Systems, Scientific Journal of Riga Technical University 29 (2011) 87-94.

[21] A. Blinov, A. Andrijanovitš, New DC/DC Converter for Electrolyser Interfacing with Stand-Alone Renewable Energy System, Electrical, Control and Communication Engineering (2012) 24-29.

[22] P. Chandrasekhar, S. Rama Reddy, Performance of Soft-Switched DC-DC Resonant converter for Electrolyzer, in: Proceedings of 4th IEEE International Symposium on Resilient Control Systems (ISRCS) (2011) 95-100.

[23] K. Viswamohan, G. Jayakrishna, Soft-Switching Techniques for DC-to-DC Converters in Electrolyzer Application, International Journal of Advanced Technology and Innovative Research 6 (9) (2014) 1021-1026.

[24] D.S. Gautam, A.K.S. Bhat, A Comparison of Soft-Switched DC-to-DC Converters for Electrolyzer Application, IEEE Transactions on Power Electronics 28 (1) (2013) 54-63.

[25] R.S. Rajesh babu, J. Henry, A comparative Analysis of DC-DC Converters for Renewable Energy System, in: Proceedings of the International MultiConference of Engineers and Computer Scientists (IMECS) (2012) 1-6.

519 [26] R. Pittini, Z. Zhang, M.A.E. Andersen, Isolated full-bridge boost DC-DC converter designed for bidirectional operation of
520 fuel cells/electrolyzer cells in grid-tie applications, in: Proc. Of 15th European Conference on Power Electronics and
521 Applications (EPE) (2013) 1-10.
522 [27] C. Cavallaro, F. Chimento, S. Musumeci, C. Sapuppo, C. Santonocito, Electrolyser in H2 Self-Producing Systems
523 Connected to DC Link with Dedicated Phase Shift Converter, in: Proc. Of IEEE International Conference on Clean Electrical
524 Power (ICCEP) (2007) 632-638.
525 [28] P. Shandrasekhar, S. Rama Reddy, Design of LCL Resonant Converter for Electrolyser, The Annals of "Dunarea de Jos"
526 University of Galati 33 (1) (2010) 5-11.
527 [29] J.C. Mayo-Maldonado, J.E. Valdez-Resendiz, V.M. Sanchez, J.C. Rosas-Caro, A. Claudio-Sanchez, F.C. Puc, A novel
528 PEMFC power conditioning system based on the interleaved high gain boost converter, International Journal of Hydrogen
529 Energy (2018), ISSN 0360-3199, https://doi.org/10.1016/j.ijhydene.2018.11.090.
530 [30] A. Garrigós, D. Marroquí, A. García, J.M. Blanes, R. Gutiérrez, Interleaved, switched-inductor, multi-phase, multi-device
531 DC/DC boost converter for non-isolated and high conversion ratio fuel cell applications, International Journal of Hydrogen
532 Energy (2018) ISSN 0360-3199, https://doi.org/10.1016/j.ijhydene.2018.11.094.
533 [31] N. Mohan, T. M. Undeland, W. P. Robbins, Power Electronics. Converters, applications and design, 3rd edition, Wiley
534 (2003).
535 [32] K. Ogata, Modern Control Engineering, 5th Edition, Prentice Hall, New Jersey, 2010.
536